JOURNAL OF PROPULSION AND POWER
Vol. 15, No. 4, July–August 1999

Unified Computer Model for Predicting Thermochemical Erosion in Gun Barrels

S. Sopok,* P. O'Hara,† and G. Pflegl†
U.S. Army Benet Laboratories, Watervliet, New York 12189
and
S. Dunn,‡ D. Coats,§ and G. Nickerson¶
Software and Engineering Associates, Inc., Carson City, Nevada 89701

A gun-barrel thermochemical erosion modeling code is presented. This modeling code provides the necessary missing element needed for developing a generalized gun-barrel erosion modeling code that can provide analysis and design information that is unattainable by experiment alone. At the current stage of code development, single-shot comparisons can be made of either the same gun wall material for different rounds or different gun wall materials for the same round. This complex computer analysis is based on rigorous scientific thermochemical erosion considerations that have been validated in the reentry nose-tip and rocket nozzle community over the last 40 years. The 155-mm M203 Unicannon system example is used to illustrate the five module analyses for chromium and gun steel wall materials for the same round. The first two modules include the gun community interior ballistics (XNOVAKTC) and nonideal gas thermochemical equilibrium (BLAKE) codes. The last three modules, significantly modified for gun barrels, include the rocket community mass addition boundary layer (TDK/MABL), gas-wall chemistry (TDK/ODE), and wall material ablation conduction erosion (MACE) codes. These five module analyses provide recession, temperature, and heat-flux profiles for each material as a function of time and axial position. In addition, the output can be coupled to finite element cracking codes. At the peak heat load axial position, predicted single-shot thermochemical wall erosion showed that both interfacial and exposed surface gun steel eroded more than 1×10^6 times faster than chromium. For chromium-plated gun steel, with its associated crack profile, it appears that interfacial gun steel degradation at the chromium crack walls leaves unsupported chromium, which is subsequently removed by the high-speed gas flow.

Nomenclature

B_a = thermochemical ablation potential
C_{cg} = mass fraction of condensed phase products
C_g = mass fraction of gas edge
Ch_b = Stanton number with blowing
Ch_0 = Stanton number without blowing
C_{pg} = mass fraction of product gas
C_w = mass fraction of wall material
H_{film} = film coefficient
H_{gw}, H_{wg} = gas–wall enthalpy
H_r = recovery enthalpy
H_w = wall enthalpy
h = molecular diffusion of gas into boundary layer
Le = Lewis number
$\dot{M}_g$ = gas mass transfer rate
M_w = molecular weight
M_{we} = molecular weight of inviscid core at edge of boundary layer
M_{wi} = molecular weight of injected gas
P, P_g = gas pressure
Q_{cw} = cold wall heat flux
$\dot{Q}$ = wall heat flux
Q_{hw} = hot wall heat flux
r_e = edge density
S = recession
$\dot{S}$ = recession rate
T_d, T_{diff} = diffusion limiting temperature
T_g = gas temperature
T_r, T_{react} = reaction limiting temperature
T_w = wall temperature
t = time
U_e = edge velocity
V_g = gas velocity
x = axial position
Z = compressibility

Presented as Paper 95-2440 at the AIAA/ASME/SAE/ASEE 31st Joint Propulsion Conference, San Diego, CA, 10–12 July 1995; received 6 August 1998; revision received 30 November 1998; accepted for publication 5 December 1998.

*Research Chemist. Member AIAA.
†Mechanical Engineer.
‡Vice President. Member AIAA.
§President. Member AIAA.
¶Retired President. Member AIAA.

Introduction

THE field of aerothermochemistry is the study of chemical reactions in flow systems and was first described by von Karman.[1] He introduced a fundamental approach to laminar flame initiation, propagation, and combustion in and around sonic and hypersonic boundary layers with reacting chemical flows. The modification of the heat transfer coefficient by a blocking effect for the mass addition of chemically reacting wall material into the boundary layer was first described by Reshotko and Cohen[2] and Cohen et al.[3] The thermochemical erosion of reentry vehicle (RV) heat shield material for various chemically reacting systems was first studied by Denison and Dooley.[4] RVs experience high temperatures and pressures, including nonlinear mass addition to the boundary layer (blowing) and shocks. The thermal protection system requires subliming or ablating heat-shield protection, whereby the increased blowing results in decreased heat transfer.

Denison and Dooley's[4] analysis regarding convective heat transfer with mass addition and chemical reactions was subsequently unified and summarized by Lees.[5] Lees's paper explained in a straightforward manner the assumptions required to solve the thermochemical erosion problem with the tools available at that time. In fact, the test of time has demonstrated that the major assumptions in Lees's paper are still reasonable and valid. Initially, Lees's

thermochemical erosion analysis model was successfully applied to external flows such as RV thermal protection systems, i.e., RV nose-tips.

Many recently declassified or unclassified experimental and analytical programs in the rocket community were spawned from Lees's work and led to the development of a number of thermochemical ablation and mechanical erosion computer models for predicting the RV nose-tip performance and the recession.[6–16]

Later, Lees's thermochemical erosion analysis model was successfully applied to internal flows associated with chemical rocket systems. Although the chemistry associated with rocket engines is considerably different than the RV environment, the analysis techniques were basically the same. Again, Lees's work led to the development of a number of thermochemical ablation and mechanical erosion computer models for predicting rocket chamber/nozzle performance and recession.[17–25]

In the last 20 years, gun-barrel technology has primarily focused on mechanical and metallurgical aspects with a secondary focus on erosion. Catastrophic gun-barrel failures have been nearly eliminated, whereas thermochemical erosion (thermochemical ablation with mechanical erosion) problems have intensified because of performance requirements demanding the use of high flame temperature propellants. The erosion of gun barrels is generally attributed to both thermal ablation (bore surface melting of unprotected gun steel/gun steel oxides with aerodynamic flow removal) and chemical ablation [gas-wall (interface and surface) chemical interaction of protected gun steel with removal of material by high-speed flow]. If the surface/interfacial temperature remains below the solidus temperature, as a practical gun design should, the primary erosion mechanism is chemical ablation. If the temperature rises above the solidus temperature, both chemical and thermal ablation may contribute to erosion. In 1990, the U.S. Army Benet Labs (Benet) Thermal Management Team identified the need for the development of a unified modeling code for predicting thermochemical erosion in gun barrels. An extensive literature search of military, NASA, and commercial sources revealed that there were no thermochemical erosion modeling codes for gun barrels. This search did reveal the two-dimensional kinetics nozzle performance (TDK) with chemistry/mass addition boundary-layer (MABL) modules and the materials ablation conduction erosion (MACE) modeling codes that work together to predict thermochemical ablation with mechanical erosion in rocket chambers, throats, and nozzles.[26,27] Since the dawn of the space-age, the TDK/MACE codes and their predecessors[7–10,14–25] have been used for rocket performance and nozzle erosion predictions. The U.S. Army's BLAKE compressible thermochemical equilibrium and XNOVAKTC interior ballistics codes[28,29] provide the necessary input for the TDK/MACE thermochemical erosion analysis of gun barrels.

The TDK/MABL module uses a simple backward-difference implicit integration method to calculate the flow variables, whereas the chemical relaxation equations are integrated using a first-order implicit integration method to ensure numerical stability in near-equilibrium flows. The code calculates flows with mass addition at the wall (blowing), transport properties, heat transfer, quasi-steady-state H_{gw}, and Mollier chart gas properties. Modifications to TDK/MABL include real gas binary mixture chemistry, finite rate chemical kinetics, generalized chemical equilibrium, a fully implicit back-difference subroutine, and linkage files to MACE.

This code analyzes the propellant-wall boundary layer with a different secondary exhaust composition transpiring through the wall, and calculates the resultant boundary-layer effect. The primary and secondary flows are treated as a binary mixture, where the rate of mixing is controlled by an eddy-viscosity model. Equilibrium, frozen chemistry at an initial equilibrium composition, or finite rate kinetics can be used to govern the flow chemistry. The boundary-layer equations for the compressible turbulent flow can be derived from the time-dependent Navier–Stokes equations using the Reynolds time-averaging procedure and the usual boundary-layer order-of-magnitude assumptions. For this work, the simplified equilibrium chemistry was used, although the nonequilibrium chemistry (generalized finite rate chemical kinetics) is possible.

For TDK/MABL, the boundary-layer equations are written in a curvilinear coordinate system in which s is the wetted length along the wall and y is measured normal to it (x is axial distance measured along the centerline). It is assumed that the lateral and transverse curvature terms can be neglected, resulting in simplified conservation equations for continuity, momentum, and energy.[26]

The MACE code solves the one-dimensional heat-conduction equation, includes mechanisms that control internal decomposition, and uses an implicit Newton's method boundary condition with an explicit interior solution. Enhancements include the surface recession boundary options determined by simple conduction; constant temperature sublimation; a Munson–Spindler-type relationship (Arrhenius-type, multiple equations, primary T, secondary P); a carbon–oxygen reaction; or a generalized chemistry boundary condition (diffusion-based, thermochemical ablation). In addition to the preceding boundary conditions, the surface material may be removed by mechanical erosion, including gas flow, particulate flow, droplet flow, and boundary-layer shear stress. Up to 10 materials may be considered with heat capacities, with/without 100% contact, contact resistances, and radiation gaps at each interface. Heat blocking caused by mass injection can be either linear or nonlinear. Convective heat transfer and boundary-layer properties may be input directly or through a linkage file with a heat transfer code. Heating rates may be modified by angle of attack, surface roughness, nonisothermal wall, or protuberance heating. Material properties may be constant or vary as a function of temperature. The variable material properties may be irreversible based on maximum temperature or reversible based on current temperature. The output is written to a file that may subsequently be used as input to a plot program, thermal stress program, or a vehicle mass loss and drag (aeroheating) program. The program uses either spherical-, cylindrical-, or rectangular-specified coordinates.[27]

The MACE code calculates the actual thermochemical erosion response. The inputs include thermal properties, the Mollier table for inert wall, the Mollier table for reacting wall, mass addition parameter tables, and boundary-layer parameters.

It is the intention of this paper to introduce and outline improvements for what is believed to be the first unified thermochemical erosion modeling code for gun barrels based on Lees's thermochemical erosion analysis model for RV heat shields and rockets.[5] At this juncture, mechanical erosion effects include only high-speed gas wash flow. Future improvements required to complete the analysis are phase-dependent blowing parameters, a time-dependent boundary layer, and a master control module for automation. In addition, this code requires critical propellant-gun system-specific information built into an automated database. Specifically designed Arrhenius and combustion gas analysis testers will provide Arrhenius profiles and combustion gas constituents, respectively. Chemical erosion data will be acquired by examining the thermochemical–mechanical alloy properties, the gas–metal eroded surface products, and the gas–metal effluent products.[30–33]

In the absence of system-specific experimental test data, previous general experimental test data can be substituted. Complex chemical interactions exist between a multicomponent gas and a multicomponent alloy because the alloy components have different selective affinities for the reactive gases, and the reactive species may not diffuse at the same rate through the alloy surface scale. In addition, alloy strength is reduced as reactive gases internally dissolve/react in alloys, or an alloy component forms a low melting-point oxide that enhances erosion.[34,35]

For this 155-mm M203 Unicannon system analysis, it was necessary to use past experimental data already available in the gun community to determine the existence of thermochemical activity, thermochemical Arrhenius profiles, and thermochemical combustion gas constituents. These experimental data showed that thermomechanical effects alone, with a nonreactive (frozen chemistry) gas mixture, do not fully explain the extent of erosion in gun tubes. Therefore, it must be assumed that thermochemical effects are a significant factor. In addition, these data indicate that propellant combustion products and alloy erosion products are gun system-dependent.[36,37]

These experimental data show that although nonequilibrium conditions may exist at the gas-wall interface, equilibrium potentials from the TDK code could be used for the MACE code. This approximation is valid in the oxide scale at the metal/metal oxide and metal oxide/metal oxide interfaces,[38,39] because equilibrium exists at the high temperatures and pressures of interest.

These experimental data also show two distinctly different chemical-related gas-wall interactions for typical chemically reducing solid propellant-product steel (or chromium-plated steel) systems. The first chemical-related gas-wall interaction is the carburization of iron and chromium involving the diffusion of carbon into the metal matrix at peak gun temperatures and pressures. In this case, the carbon forms a solid solution with the iron or chromium. In this region, the metal's structure is unaltered and the metal and the carbon are two distinctly different components in physical proximity, but not chemically bound. This case describes a purely mechanical interaction and does not describe true thermochemical ablation. As the system returns to room temperature, the iron–metal matrix cannot physically retain the free carbon and precipitates physically bound carbon as chemically bound iron carbide (Fe_3C) throughout the solid-solution iron matrix. The return to room temperature also causes thermal contractions between surface austenite and carburized subsurface tempered martensite, which produces stress cracks (heat checking). This carburization effect still does not qualify as thermochemical ablation, because this phenomenon involves no material removal. This interaction is considered a degrading phenomenon, considering that the metal matrix alloy is case-hardened, has a lowered melting point, and is weakened because of cracking and mechanical erosive forces. Experimental data support the existence of gun-barrel carburization.[40–43] The melting point of gun steel is 400°C lower than the melting point of chromium. For these systems, carburization lowers the solidus melting point by 50–400°C for gun steel and 50–100°C for chromium, based on respective phase diagrams that justify chromium plating of steel.

These experimental data also show another chemical-related gas-wall interaction for typical chemically reducing solid-propellant-product steel (or chromium-plated steel) systems. This second chemical-related gas-wall interaction is the oxidation of iron and chromium. This occurs initially at the metal gas interface, then at the metal/metal oxide interface of surfaces and plated interfaces. The process involves the diffusion of oxygen from oxygen-rich gas product species into the metal at peak gun temperatures and pressures. In this case, the oxygen forms a distinct iron- or chromium-oxide scale layer. This case describes true thermochemical ablation because the brittle scale layer is highly susceptible to cracking and is easily removed by mechanical erosive forces. As the system returns to room temperature, the metal oxide retains the same chemical structure in the scale layer. Despite the possibility of nonequilibrium at the gas-wall interface, experimental data and chemical equilibrium codes indicate the near exclusive presence of iron-oxide or chromium-oxide metal–gas compound products when exposed to the combustion products. Typically, these chemically reacting gases require approximately a 50% increase in molar oxygen to obtain complete product combustion to carbon dioxide and water. Experimental data support the existence of gun-barrel oxidation.[44–50] For these systems, oxidation lowers the melting point by 100–200°C for gun steel, and raises the melting point by 400–500°C for chromium, based on respective phase diagrams that further justify the chromium plating of steel.

Procedure

The 155-mm M203 Unicannon gun system thermochemical erosion analysis procedure consists of five analyses, utilizing the NOVA, BLAKE, TDK/MABL, TDK/ODE, and MACE codes. The NOVA interior ballistics analysis outputs boundary-layer edge conditions for gas pressure, velocity, and temperature as a function of position and time. The BLAKE gas thermochemical equilibrium analysis outputs pressure/temperature temporal states and compressibility tables. The TDK/MABL boundary-layer mass addition analysis outputs recovery enthalpy and heat transfer data. The TDK/ODE gas-wall thermochemical equilibrium analysis outputs inert/reacting wall enthalpies and blowing parameters. The MACE ablation, erosion, and temperature profile analysis outputs surface/in-wall temperature and erosion profile data. All cases start at ambient conditions and are for a single shot.

The NOVA code interior ballistics analysis includes the 22-ft cannon with a 0.020-s in-bore phase, the M203 charge, the 26-lb M30A1 propellant, and the 96-lb M549 projectile. The M30A1 propellant consists of 28% nitrocellulose, 22% nitroglycerine, 47% nitroguanidine, 1% ethyl centralite, 1% potassium sulfate, and 1% other minor species. The NOVA code calculates the time-dependent flowfield, and evaluates the maximum and minimum state variables. The results of the NOVA calculations may be considered the input to the entire erosion analysis. The NOVA input file follows the format given in the NOVA user's manual.[29] This file contains gun system-specific data not included within the NOVA code. NOVA outputs gas pressure (psi), gas velocity (ft/s), gas temperature (R), and film coefficient (Btu/in.^{2} s °R) data at the wall. At 12 preselected axial locations, separate files were generated that contained the preceding data as a function of time. A file generation utility code is used to convert the 12 axial location NOVA output files (with pressure, velocity, temperature, and density vs time) into 12 preselected time slice linkage files (with pressure, velocity, temperature, and density vs axial distance), with the format required by the TDK/MABL analysis module. Although this is an extremely limited sampling, the time factor and the meticulous nature of linking up the different modules necessitate this approach. These files contain boundary-layer edge conditions that will be used by the TDK/MABL code to calculate heat transfer parameters.

The BLAKE thermochemical equilibrium analysis evaluates the maximum and minimum state variable ranges identified by the NOVA output. The BLAKE input file follows the format given in the BLAKE user's manual.[28] This file contains the M30A1 chemistry and state variable ranges. BLAKE was modified to output chemical composition and compressibility (dense gas correction) linkage file data at the 12 axial locations as a function of NOVA temperature and pressure variations. These files were subsequently used to calculate gas properties by the TDK/MABL and TDK/ODE modules.

The TDK/MABL analysis calculates the boundary-layer characteristics with the edge properties extracted from the 12 NOVA preselected time-slice linkage files (with pressure, velocity, temperature, and density vs axial location) and BLAKE linkage file (chemical composition and compressibility vs temperature and pressure). The boundary-layer module calculates adiabatic conditions and the cold wall heat transfer rate, using the previous files as input. The TDK/MABL analysis first calculates the adiabatic condition ($q_{hw} = 0$) and then calculates the cold wall condition (T_{wall} and H_{wall}, both are constant), resulting in a total of 24 analyses. The TDK/MABL analysis requires 24 input files (12 adiabatic and 12 cold wall), where each includes chemistry and compressibility for the applicable state variable ranges. These adiabatic and cold wall input files follow the format given in the TDK user's manual.[26] The TDK/MABL code internally generates transport properties and Mollier gas properties for each analysis, and these data are used to calculate the boundary-layer characteristics. TDK/MABL generates 24 output files with adiabatic conditions, and heat transfer rates, which are subsequently used to tabulate time-dependent boundary-layer properties at two selected locations, the 1- and 2-ft axial stations.

The TDK/ODE analysis requires eight cases including 1) nonreacting inert wall with no omitted species; 2) nonreacting inert wall with omitted condensed species C(GR); 3) reacting chromium wall with no omitted species; 4) reacting chromium wall with omitted species C(GR), CR_2N(S), and CRN(S); 5) reacting gun steel wall with no omitted species; 6) reacting gun steel wall with omitted species C(GR); 7) reacting iron wall with no omitted species; and 8) reacting iron wall with omitted species C(GR). All of these cases include the BLAKE chemical composition and compressibility (function of temperature and pressure) linkage file data. In cases 3–8, the solid propellant combustion products are totally saturated with an excess of the wall material. Product omissions are based

on Ref. 44. The eight key input files follow the format given in the TDK user's manual.[26] These files contain the M30A1 chemistry and state variable ranges. For each case, TDK/ODE outputs linkage files (Mollier charts) as a function of pressure and temperature for MACE, including 1) inert gas-wall enthalpy $(H_{gw})_{inert}$ linkage file; 2) reacting gas-wall enthalpy $(H_{gw})_{reacting}$ linkage file; and 3) chemical ablation potential (B_a) linkage file.

The MACE analysis computes the resulting thermochemical erosion response and in-depth temperature profiles. The analysis was performed for four cases, which include two chromium calculations and two gun steel calculations (both at axial locations at 1 and 2 ft). The corresponding MACE input files follow the format described in the MACE user's manual[27] and are generated from the TDK/MABL and TDK/ODE linkage data described earlier. The convective environment section, i.e., pressure, recovery enthalpy, cold wall heat transfer rate, etc., varied in the preceding files. MACE linkage file data from TDK/MABL include tabulated cold wall heating data, thermal properties, recovery enthalpy data, and transport properties data, from the 24 corresponding TDK/MABL cases. MACE linkage file data from TDK/ODE are in the form of Mollier charts, and include inert gas-wall enthalpy, reacting gas-wall enthalpy, and the chemical ablation potential for each case. MACE outputs surface erosion, surface temperature, and temperature profiles as a function of time for each case.

Results and Discussion

The current thermochemical erosion model requires input from five different analyses to compute surface recession. As an example, the AFAS 155-mm system including the M203 charge and M30A1 propellant is used. The time-dependent core flow in the gun barrel must be known. That is, the velocity, pressure, and temperature distribution in the barrel must be known as a function of time and space. For our analysis this information is considered to be a specified input. Next, the chemical composition of the gases in the barrel must also be known. Our model is based on the premise that equilibrium chemistry applies at the temperatures and pressures associated with gun-barrel interior ballistics. Equilibrium chemistry calculations are made for the combusted propellant without wall material. With the core flow properties known, the boundary-layer parameters can be calculated, again assuming chemical equilibrium. As pointed out by Lees,[5] the boundary-layer analysis can be calculated for a nonreacting wall, and modified to account for chemical reactions and mass addition. Two boundary-layer calculations are necessary for each time point evaluated, the first to calculate the cold wall heat transfer coefficient and the second to calculate the adiabatic wall temperature. Thermochemical equilibrium chemistry calculations are then made with the combusted propellant gases and reacting wall material. These calculations supply the wall mass flux (blowing rate) and wall-gas enthalpy tables needed to complete the analysis.

All of the preceding quantities are used to calculate the transient thermochemical response. For this analysis, the governing heat transfer equations are greatly simplified using Fick's law for binary diffusion. For the special case of unity Lewis number, the complete similarity between heat transfer and mass transfer is employed to solve the resulting equations. Finally, the mass addition of reacting wall material into the boundary layer modifies the heat transfer coefficient by the well-known blocking effect.[2]

The equations that govern an ablation model for convective heat transfer and mass addition to a chemically reacting boundary layer are quite difficult to solve. Fortunately, a series of physical assumptions reduces the problem, so that meaningful results can be obtained, and they include 1) one-dimensional steady-state ablation, 2) convective heat transfer based upon a constant steady-state value, 3) mass loss in the form of gas phase diffusion, 4) melt runoff where the melt layer is assumed to be infinitesimally thin, 5) complete species diffusion in the melt layer, 6) no species diffusion in the solid phase, 7) melt layer obeying a prescribed phase diagram for composition vs temperature, 8) diffusion-controlled combustion; 9) unity Lewis and Prandtl numbers; and 10) equilibrium chemistry.[12]

Thermochemical ablation involves surface and interfacial reacting flow, ablation products, diffusion, eddy turbulence, radiation, gas-wall reaction zone, heat transfer, mass transfer, temperature gradients, thermal stress cracking, microcrack erosion, melting layer, and mechanical removal. The ablation model employed in this analysis includes the gas, the solid wall, the melt layer, heat transfer by convection and radiation, surface temperature effects, mass transfer at the gas-wall interface, enthalpy at the gas-wall interface, and mechanical erosion. Ablation products include all material coming off the wall, in gas, solid, and liquid phases. Blowing is gas coming off the wall and diffusing into the boundary layer.

The two types of thermochemical ablation modeling available are the engineering approach and the Navier–Stokes approach. This paper focuses on the engineering approach, whereas the Navier–Stokes approach will be addressed in a future paper. The engineering model includes decoupled fluid flow (boundary layer and inviscid core), interior ballistics, boundary-layer heat transfer, and thermal response analysis. This analysis also assumes equilibrium chemistry for ablation, unity Lewis and Prandtl numbers, and similarity between heat and mass transfer.

Engineering approach modeling is relatively straightforward, whereby each mechanism's importance is identified, modest computer resources are needed, parametric analysis is possible, and incremental module upgrades are feasible. However, this approach requires engineering judgment, and extrapolations may be questionable.

The engineering approach core assumptions include 1) test data support unity Lewis number (with similarity existing between heat and mass transfer); 2) the computed chemical ablation potential B_a values, which can be calculated from equilibrium chemistry; 3) immediate molecule-wall reactions forming equilibrium products; 4) second-order importance of reacting chemistry on the blowing potential and heat transfer interaction; 5) the concept of a boundary layer; and 6) the concept of an inviscid core.

Figures 1–4 show NOVA travel and time vs pressure, velocity, temperature, and film coefficient data for the 155-mm M203 gun system for TDK/MABL input. For the entire NOVA/BLAKE/TDK/MACE analysis, all unknown parameters can be determined by experiment. Incidentally, NOVA-predicted energy loss order is highest for the gas, then for the projectile, and then for the tube.

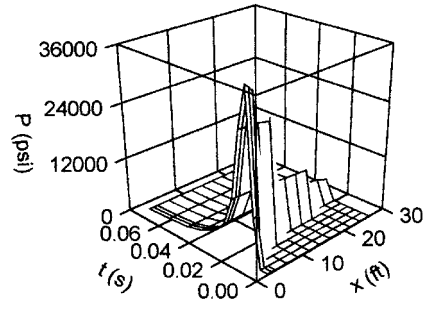

Fig. 1 Nova gas pressure data as functions of time and position.

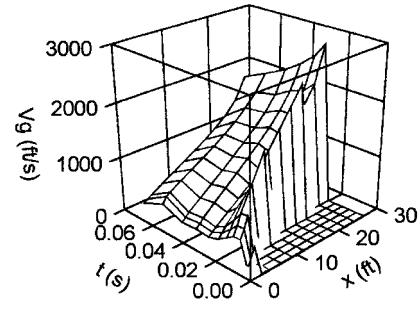

Fig. 2 Nova gas velocity data as functions of time and position.

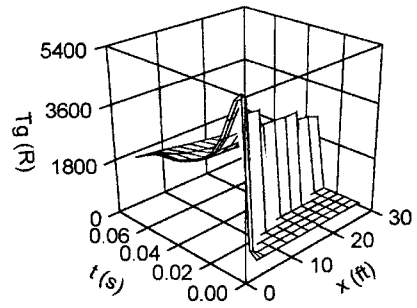

Fig. 3 Nova gas temperature data as functions of time and position.

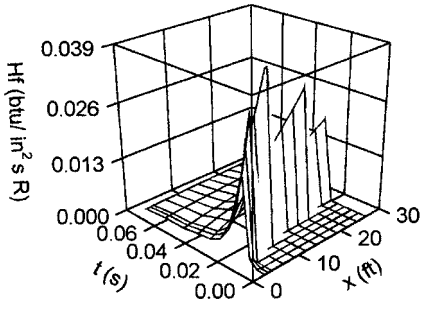

Fig. 4 Nova film coefficient data as functions of time and position.

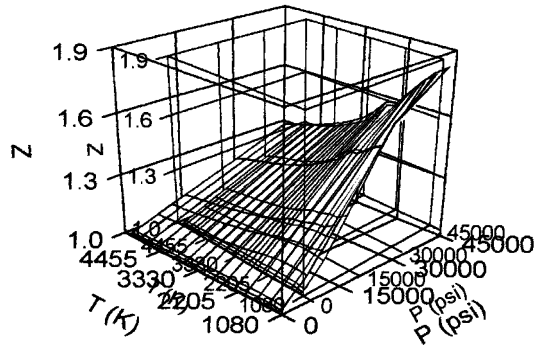

Fig. 5 Blake compressibility data as functions of pressure and temperature.

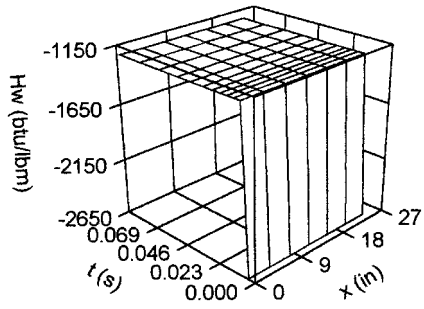

Fig. 6 TDK/MABL wall enthalpy data as functions of time and position.

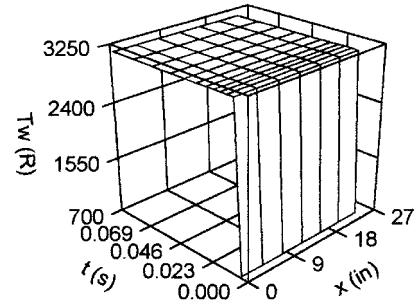

Fig. 7 TDK/MABL wall temperature data as functions of time and position.

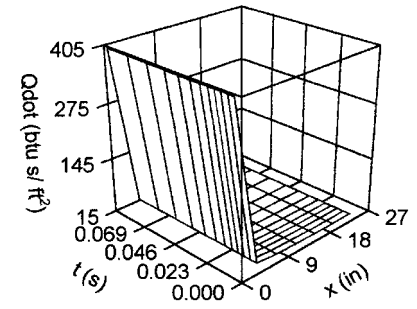

Fig. 8 TDK/MABL heat flux data as functions of time and position.

Figure 5 plots BLAKE pressure–temperature–compressibility data for the 155-mm M203 gun system for TDK/MABL and TDK/ODE input. BLAKE thermochemical equilibrium products are confirmed by unpublished in-house experimental Arrhenius testing, experimental combustion gas analysis, and past experimental data for combustion product species.

The TDK/MABL analysis is the weak link in the total erosion analysis because it does not include time-dependent effects. The resulting 155-mm M203 gun system TDK/MABL output data are subsequently used for MACE code input. Figure 6 plots the TDK/MABL axial location–time–adiabatic wall enthalpy data. The recovery enthalpy at the adiabatic wall temperature H_r is the potential chemistry driver where the heat transfer approaches zero. Figure 7 plots the TDK/MABL axial location–time–adiabatic wall temperature data. This temperature T_{aw} is the potential temperature without reactions. Figure 8 plots the TDK/MABL axial location–time–cold wall heat transfer rate data. This heat flux Q_{cw} is the wall heat flux evaluated at the cold wall temperature. The plots of the TDK/MABL output indicate that the peak heat load was located ~1–2 ft from the breech. Therefore, the boundary-layer parameters (recovery enthalpy and cold wall heat transfer rate) were extracted from the TDK/MABL output as a function of time at the 1- and 2-ft locations for MACE code input. The TDK/MABL analysis shows that guns add only a small amount of mass to the boundary layer, which thickens it, and decreases heat transfer conduction to the wall.

The TDK/MABL heat and mass transfer model includes the following three equations, For mass addition to the boundary layer:

$$r_e U_e C h_0 = \frac{Q_{cw}}{H_r - H_{gw}} \tag{1}$$

For the heat-to-mass transfer ratio:

$$r_e U_e C h_b = \dot{M}_g / B_a, \qquad Le = 1 \tag{2}$$

For the overall correlation between these two equations:

$$\frac{Ch_b}{Ch_0} = f(B_a, M_w) = 1 - \frac{h\dot{M}_g}{r_e U_e C h_0} \tag{3}$$

where $h = a(M_{we}/M_{wi})^{**b}$, h is related to the molecular diffusion of the gas into the boundary layer, a is the coefficient, and b is the exponent.

For a description of the TDK/ODE analysis, see Ref. 17. The following 155-mm M203 gun system TDK/ODE output data are for

MACE code input. Figure 9 plots TDK/ODE pressure–temperature–inert H_{gw} data for chromium. Figure 10 plots TDK/ODE pressure–temperature–reacting wall H_{gw} data for chromium. Figure 11 plots TDK/ODE pressure—temperature–C_{cg} data (transposed) for chromium. Figure 12 plots TDK/ODE pressure–temperature–B_a data (transformed) for chromium. Figure 13 plots TDK/ODE pressure–temperature–inert H_{gw} data for gun steel. Figure 14 plots TDK/ODE pressure–temperature–reacting wall H_{gw} data for gun steel. Figure 15 plots TDK/ODE pressure–temperature–C_{cg} data (transposed) for gun steel. Figure 16 plots TDK/ODE pressure–temperature–B_a data (transformed) for gun steel.

Choosing chemical equilibrium species requires considerable experience: Experimental data or chemical kinetic analysis determine if species should be omitted because of kinetic blocking.

The reaction-limiting temperature T_{react} is the onset temperature of the exothermic reaction for a given pressure, whereas the

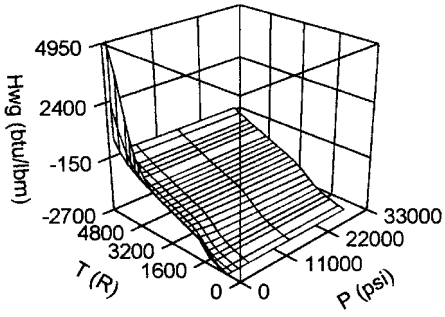

Fig. 9 TDK/ODE enthalpy of the inert gas-wall data as functions of pressure and temperature.

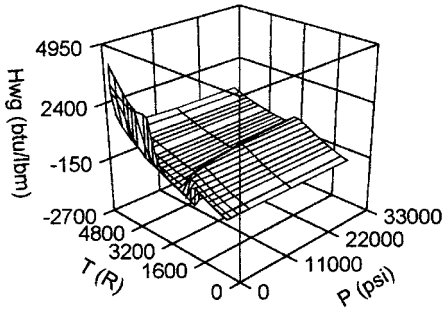

Fig. 10 TDK/ODE enthalpy of the reacting gas-chromium wall data as functions of pressure and temperature.

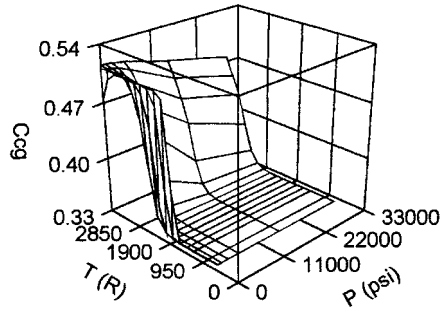

Fig. 11 TDK/ODE chromium condensed-phase products mass fraction data as functions of pressure and temperature.

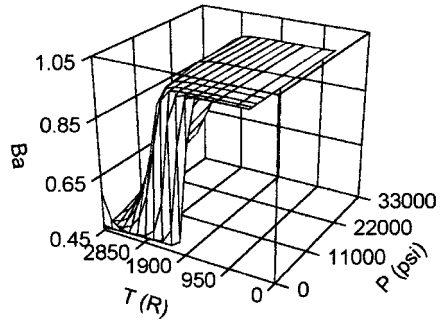

Fig. 12 TDK/ODE chromium thermochemical ablation potential data as functions of pressure and temperature.

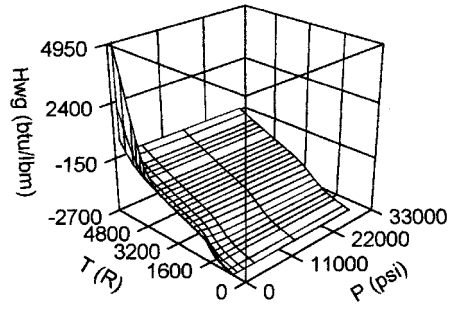

Fig. 13 TDK/ODE enthalpy of the inert gas-wall data as functions of pressure and temperature.

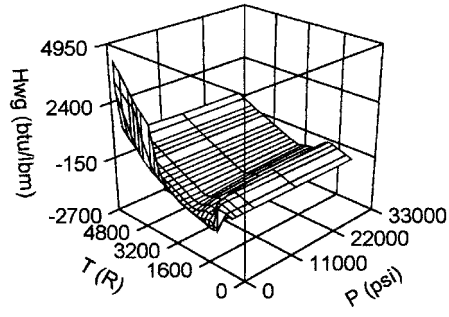

Fig. 14 TDK/ODE enthalpy of the reacting gas-gun steel wall data as functions of pressure and temperature.

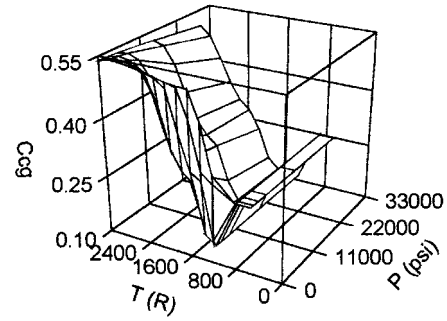

Fig. 15 TDK/ODE gun steel condensed phase products mass fraction data as functions of pressure and temperature.

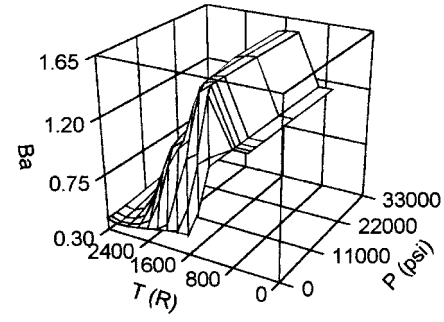

Fig. 16 TDK/ODE gun steel thermochemical ablation potential data as functions of pressure and temperature.

diffusion-limiting temperature T_{diff} is the diffusion-limited equilibrium temperature point of the exothermic reaction for a given pressure. One way to determine T_{react} and T_{diff} is by an Arrhenius tester that provides gas-wall reaction data as a function of pressure and temperature. Another way is by using a time-dependent chemical kinetics code. For the purpose of this work, the chromium and gun steel data are acquired from Figs. 10 and 14, respectively. Figure 10 chromium data includes respective $P(\text{psi})-T_{\text{react}}(^\circ\text{R})-T_{\text{diff}}(^\circ\text{R})$ triplets of 10–1800–2200; 100–2000–2400; 1000–2350–2800; 2500–2400–3000; 5000–2600–3000; 15,000–2800–3200; and 30,000–3000–3400. The gun steel data in Fig. 14 includes respective $P(\text{psi})-T_{\text{react}}(^\circ\text{R})-T_{\text{diff}}(^\circ\text{R})$ triplets of 10–800–1600; 100–1150–2000; 1000–1200–2400; 2500–1350–2600; 5000–1400–2800; 15,000–1550–3000; and 30,000–1600–3000.

The TDK/ODE ablation model assumes that as the gas diffuses to the wall/interface, it reacts to form equilibrium products as follows:

$$B_a = (C_w - C_{cg})/C_g = (C_{pg} - C_g)/C_g \tag{4}$$

where C_{cg} is counted on the wall surface/interface, not counted off the wall surface/interface.

Figure 11 shows C_{cg} [Cr(s) mass fraction] with respect to pressure and temperature. At gun pressures with a gas oxidizer–chromium fuel ratio (O/F) of 0.5, Cr(s) is in equilibrium with Cr_2O_3(s) from ambient temperature up to its metal melting temperature (3800–4000°R). In Fig. 11, C_{cg} [mass fraction of Cr(s) before reaction onset] equals 0.3373 at gun conditions. By definition, C_w is the percent fuel $= 1.0/1.5 = 0.6667$ and C_g is the percent gas $= 1 - C_w = 0.3333$. Figure 12 shows B_a as a function of gun pressure and temperature, where $B_a = (C_w - C_{cg})/C_g = 0.991$ and is required for MACE input.

This chromium case was run for $O/F = 0.1$, $C_w = 0.9091$, $C_g = 0.0909$, $C_{cg} = 0.819$, and $B_a = 0.991$; and it shows that B_a is independent of gun pressures and O/F, but is very dependent on stoichiometry. B_a is fixed by chosen reactant and product stoichiometry. Both B_a and C_{cg} are chosen here where the solid (sol) metal starts to react, although experimental data would be a better approach. C_{cg} uses only the metal (sol) and not the liquid (liq) metal or metal (gas).

Figure 15 shows C_{cg} for the gun steel (sol) mass fraction with respect to pressure and temperature. The computations show that C_{cg} for gun steel was nearly identical to C_{cg} for iron, most likely because iron comprises ~95% of gun steel. For the purposes of this paper, C_{cg} for iron is used to illustrate these results, although this same illustration is true for the other gun steel metals, which add only a very minor correction. At gun pressures with an O/F of 0.5, Fe(A) is in equilibrium with Fe_3O_4(s) from ambient to 1000°R, Fe(A) is in equilibrium with FeO(s) from 1000 to 2100°R, Fe(C) is in equilibrium with FeO(s) from 2100 to 2900°R, and Fe(D) is in equilibrium with FeO(L) from 2900 to its metal melting temperature (3200 to 3400°R). Fe(s) is a combination of Fe(A), Fe(C), and Fe(D). The literature[44] shows that the equilibrium of Fe(A) with Fe_3O_4(s) from ambient to 1000°R does not exist and that it is all Fe(A). Thus, in Fig. 15, C_{cg}, which is the mass fraction of Fe(s) before reaction onset, equals 0.136 at gun conditions. Again, by definition, C_w is percent fuel $= 1.0/1.5 = 0.6667$, and C_g is percent gas $= 1 - C_w = 0.3333$. Figure 16 shows B_a as a function of gun pressure and temperature, where $B_a = (C_w - C_{cg})/C_g = 1.59$ and is required for MACE input.

The iron case was run for $O/F = 0.1$, $C_w = 0.9091$, $C_g = 0.0909$, $C_{cg} = 0.7646$, and $B_a = 1.59$; and again it shows that B_a is independent of gun pressures, independent of O/F, but very dependent on stoichiometry. Again, the following is true: B_a is fixed by chosen reactant and product stoichiometry, both B_a and C_{cg} are chosen where metal(s) starts to react, although experiment would be better, and C_{cg} uses only the metal (sol) and not the metal (liq) or metal (gas).

The TDK/ODE thermochemical equilibrium products are confirmed by experimental Arrhenius testing (thermal analysis), experimental combustion gas analysis for metal products (gas chromatography, mass spectrometry, x-ray diffraction), experimental surface analysis for metal products (Auger spectrometry, ESCA spectrometry), and past experimental data for combustion product species. Combustion gas analysis shows that metallic combustion products generally quench to the same metal products. This analysis calls on experience and is difficult to automate.

TDK/ODE may zero out the negative B_a values above the melt temperature of the wall material. Although this requires refinement, it does not affect this analysis because melted material is instantly removed, by definition.

It should be noted that the TDK/ODE thermochemical equilibrium calculations, which generated B_a and H_{gw} tables, included the effects of complex chemical reactions, vaporization, melting, and metal alloys.

TDK has equilibrium, kinetics, and frozen chemistry options. The TDK/ODE chemical equilibrium option is used for this work and predicts maximum recession. Therefore, this option is very useful from a gun-design standpoint. The TDK/ODK finite rate chemical kinetics Arrhenius-type option predicts actual recession. Unfortunately, this option was not used for this analysis, because this module currently lacks sufficient input data for it to be a practical tool. The TDK/ODE frozen chemistry option predicts no recession, and was not used here except to show that erosion does have a chemical component.

In summary, the TDK/ODE chemical equilibrium option was chosen because it is a practical approximation of gun-barrel interior ballistics chemistry, where sufficient activation energy coupled with many collisions generates fast reaction rates, high temperature, and high pressure for the given time frame.

The following 155-mm M203 gun system MACE output data predict surface erosion, surface temperature, and temperature profiles for each axial location case. Figure 17 plots these MACE T_{react}–time–recession (S) data for chromium at station 1. Figure 18 plots these MACE T_{react}–time–recession rate ($\dot{S}$) data for chromium at station 1. Figure 19 plots these MACE T_{react}–time–cold wall heat transfer rate (Q_{cw}, cold wall heat flux) data for chromium at station 1. Figure 20 plots these MACE T_{react}–time–hot wall heat transfer rate (Q_{hw}, hot wall heat flux) data for chromium at

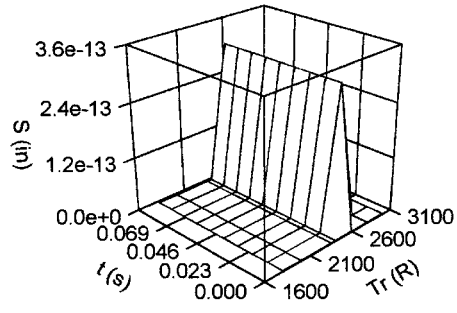

Fig. 17 MACE station 1 chromium recession data as functions of reaction limiting temperature and time.

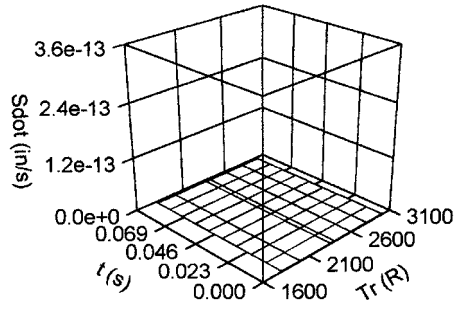

Fig. 18 MACE station 1 chromium recession rate data as functions of reaction limiting temperature and time.

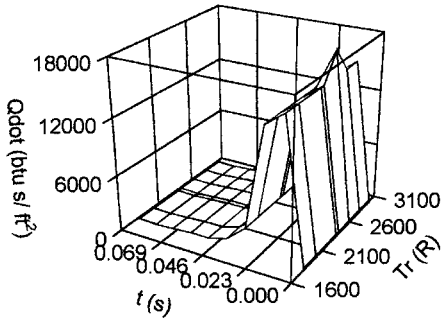

Fig. 19 MACE station 1 chromium cold wall heat flux data as functions of reaction limiting temperature and time.

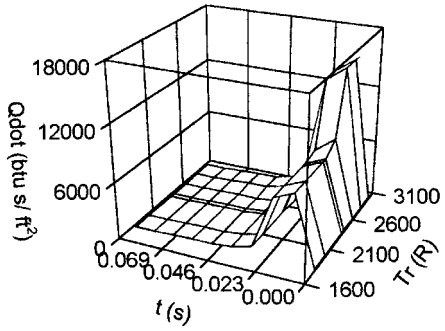

Fig. 20 MACE station 1 chromium hot wall heat flux data as functions of reaction limiting temperature and time.

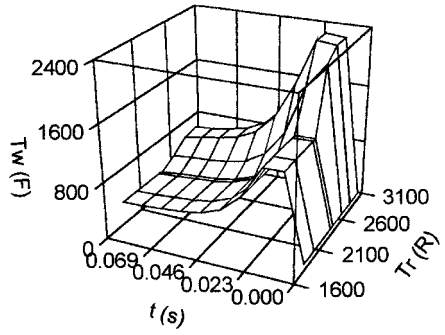

Fig. 21 MACE station 1 chromium wall temperature data as functions of reaction limiting temperature and time.

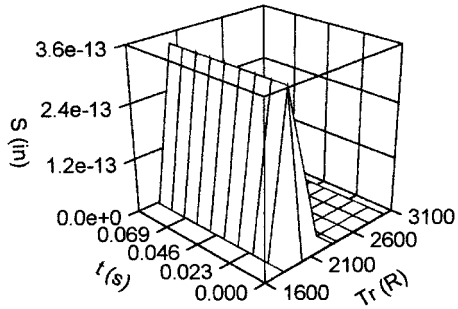

Fig. 22 MACE station 2 chromium recession data as functions of reaction limiting temperature and time.

station 1. Figure 21 plots these MACE T_{react}−time−wall temperature (T_{wall}) data for chromium at station 1. Figure 22 plots these MACE T_{react}−time−recession (S) data for chromium at station 2. Figure 23 plots these MACE T_{react}−time−recession rate ($\dot{S}$) data for chromium at station 2. Figure 24 plots these MACE T_{react}−time−cold wall heat transfer rate (Q_{cw}) data for chromium at station 2. Figure 25 plots these MACE T_{react}−time−hot wall heat transfer rate (Q_{hw}) data for chromium at station 2. Figure 26 plots these

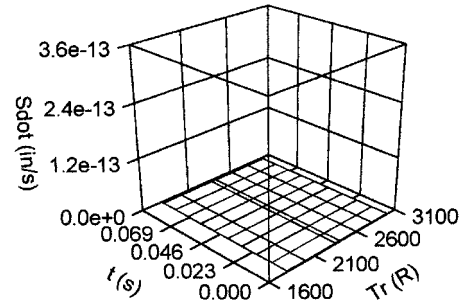

Fig. 23 MACE station 2 chromium recession rate data as functions of reaction limiting temperature and time.

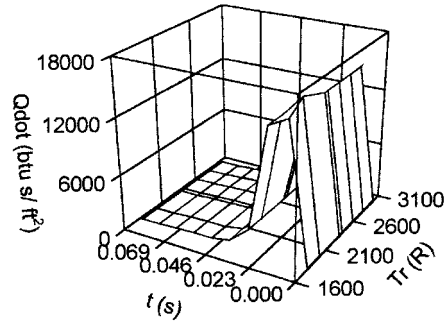

Fig. 24 MACE station 2 chromium cold wall heat flux data as functions of reaction limiting temperature and time.

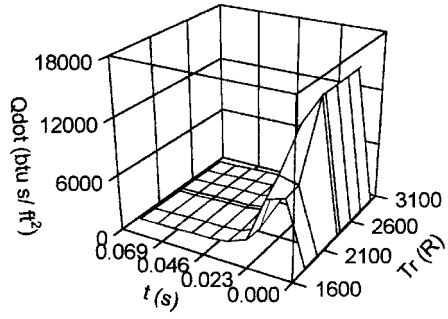

Fig. 25 MACE station 2 chromium hot wall heat flux data as functions of reaction limiting temperature and time.

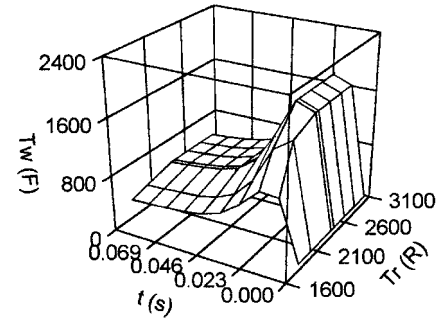

Fig. 26 MACE station 2 chromium wall temperature data as functions of reaction limiting temperature and time.

MACE T_{react}−time−wall temperature (T_{wall}) data for chromium at station 2.

Figures 17–26 predict that the chromium at stations 1 and 2 are nearly inert to thermal and thermochemical erosion because of insufficient heat transfer/wall temperatures to achieve chromium reaction temperatures, insufficient heat transfer/wall temperatures to achieve the chromium transformation temperature, insufficient heat transfer/wall temperatures to achieve the chromium melting temperature, and extremely small erosion/erosion rates.

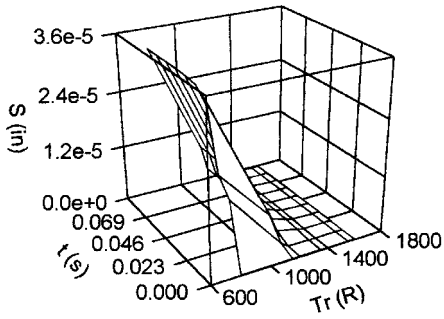

Fig. 27 MACE station 1 gun steel recession data as functions of reaction limiting temperature and time.

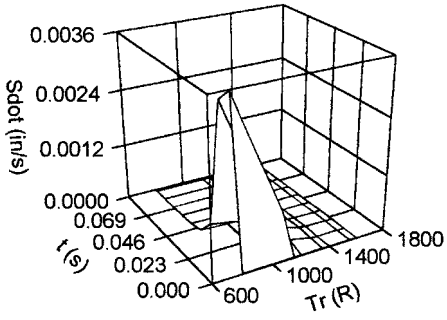

Fig. 28 MACE station 1 gun steel recession rate data as functions of reaction limiting temperature and time.

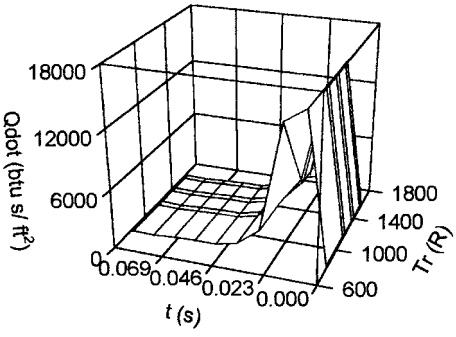

Fig. 29 MACE station 1 gun steel cold wall heat flux data as functions of reaction limiting temperature and time.

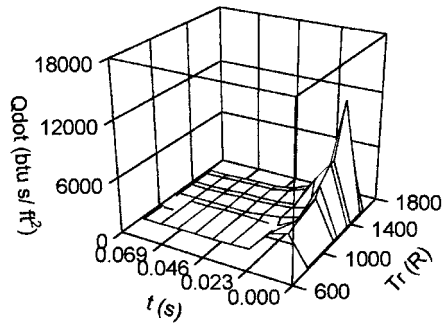

Fig. 30 MACE station 1 gun steel hot wall heat flux data as functions of reaction limiting temperature and time.

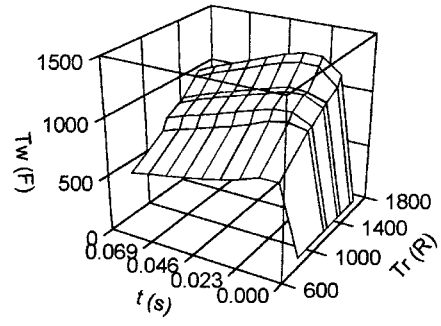

Fig. 31 MACE station 1 gun steel wall temperature data as functions of reaction limiting temperature and time.

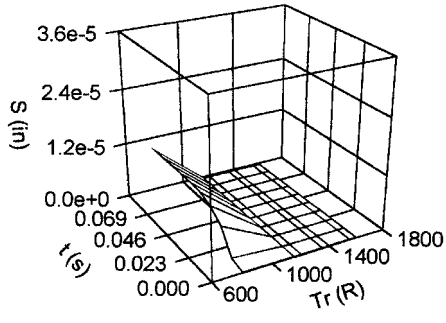

Fig. 32 MACE station 2 gun steel recession data as functions of reaction limiting temperature and time.

Figure 27 plots these MACE T_{react}−time−recession (S) data for gun steel at station 1. Figure 28 plots these MACE T_{react}−time−recession rate ($\dot{S}$) data for gun steel at station 1. Figure 29 plots these MACE T_{react}−time−cold wall heat transfer rate (Q_{cw}) data for gun steel at station 1. Figure 30 plots these MACE T_{react}−time−hot wall heat transfer rate (Q_{hw}) data for gun steel at station 1. Figure 31 plots these MACE T_{react}−time−wall temperature (T_{wall}) data for gun steel at station 1. Figure 32 plots these MACE T_{react}−time−recession (S) data for gun steel at station 2. Figure 33 plots these MACE T_{react}−time−recession rate ($\dot{S}$) data for gun steel at station 2. Figure 34 plots these MACE T_{react}−time−cold wall heat transfer rate (Q_{cw}) data for gun steel at station 2. Figure 35 plots these MACE T_{react}−time−hot wall heat transfer rate (Q_{hw}) data for gun steel at station 2. Figure 36 plots these MACE T_{react}−time−wall temperature (T_{wall}) data for gun steel at station 2.

Figures 27–36 predict that the gun steel at stations 1 and 2 are quite susceptible to thermochemical erosion because of sufficient heat transfer/wall temperatures to achieve gun steel reaction temperatures, sufficient heat transfer/wall temperatures to achieve the gun steel transformation temperature, and significant erosion/erosion rates. These figures also predict that the gun steel is not susceptible to thermal erosion as a result of insufficient heat transfer/wall temperatures to achieve the gun steel melting temperature.

The A723 melting point is 1452°C or 3106°R, and was used for MACE input as an approximation of gun steel. The chromium melting point is 1845°C or 3813°R, and was used for MACE input as an approximation of the chromium-plated surface. Density, conductivity, and specific heat data for MACE input are from the NOVA database.

The MACE calculations used the TDK/ODE tables and the TDK/MABL boundary-layer parameters for the boundary conditions. The purely equilibrium results indicate that an enormous amount of wall metal reacts with the hot gases in the boundary layer. Because the preceding analysis was for equilibrium flow, it only represents a limiting case.

Because the chemical kinetics for the gas-wall interaction has not been studied to date, the temperatures where the kinetics begin and equilibrium is achieved are parametrically stacked for each case. These f-function data can be determined experimentally with standard test techniques. An important experimental test to determine T_{react}, T_{diff}, and the cubic Arrhenius f-function is by using a thermogravimetric analyzer (TGA) or differential scanning calorimeter

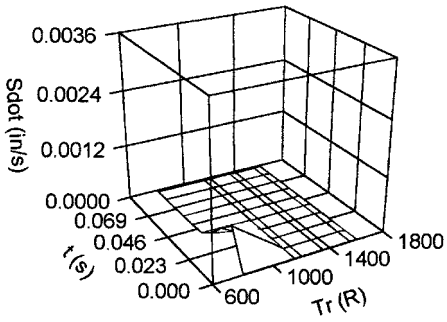

Fig. 33 MACE station 2 gun steel recession rate data as functions of reaction limiting temperature and time.

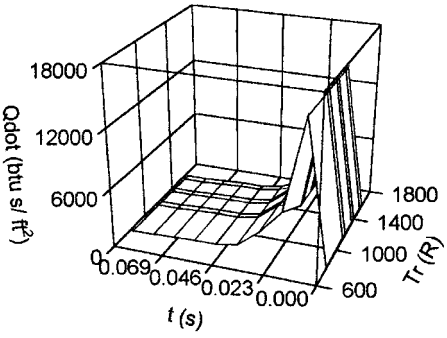

Fig. 34 MACE station 2 gun steel cold wall heat flux data as functions of reaction limiting temperature and time.

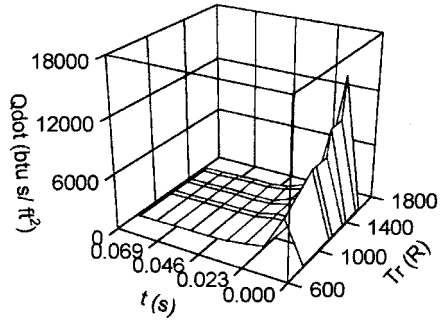

Fig. 35 MACE station 2 gun steel hot wall heat flux data as functions of reaction limiting temperature and time.

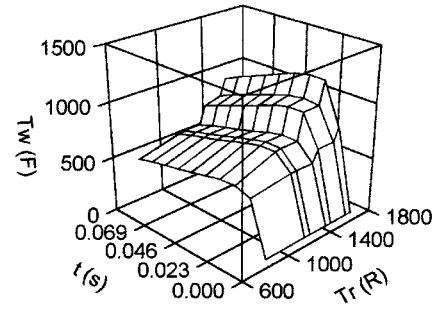

Fig. 36 MACE station 2 gun steel wall temperature data as functions of reaction limiting temperature and time.

(DSC)-type Arrhenius tester with captured combustion gases (or at least a pure gas of interest). Because reaction rate is a weak function of pressure, low-pressure flow of propellant products or pure gas can be used in a TGA (dm vs T, up to 1000°C, cubic transition curve) or a DSC (dq vs T, up to 600°C, bell-shaped curve), because the extreme sensitivity of these instruments compensates for the much-reduced pressure. The experimental Arrhenius method determines nonequilibrium (chemical kinetic) recession rates. The MACE code needs only the actual Arrhenius profile case for an exact solution.

It should be noted that an equilibrium analysis of iron and air at room temperature will show that the iron will combine with the oxygen to form iron oxides. But this reaction occurs over a time scale that is many orders-of-magnitude greater than the time scale of interest, it can be concluded that this system is not in equilibrium and therefore must be kinetically controlled. On the other hand, if the preceding system were evaluated at 5000°R (2504°C), the TDK/ODE calculations would be reasonable, and it could be concluded that the system would indeed be in equilibrium.

Although the temperatures and pressures associated with the gun-barrel interior ballistics suggest the use of an equilibrium analysis, the transient thermal response of the wall requires a kinetic wall function relating the chemistry associated with the reacting wall and inert wall. At low temperatures the wall is inert, whereas at elevated temperatures the wall chemically reacts with the propellant products. Therefore, it is assumed that there is a temperature below which no reactions occur, referred to as T_{react}. It is also assumed that there is another temperature above which the system is in complete equilibrium, referred to as T_{diff}. The final answer is still not precisely known until an ancillary kinetic study is performed to determine T_{react} and T_{diff}.

As explained in the preceding text, T_{react} and T_{diff} can be determined by an Arrhenius tester or by a proposed time-dependent chemical kinetics code. For the purpose of this work, the chromium and gun steel data used by TDK/ODE were obtained from Figs. 10 and 14, respectively. The TDK/ODE Mollier table of $(H_{gw})_{react}$ (vs temperature and pressure) provides equilibrium values for T_{react} and T_{diff} for MACE input cases. T_{react} is at the onset temperature of the exothermic reaction, and T_{diff} is at the diffusion-limited equilibrium temperature point of the exothermic reaction. These temperatures may be a weak function of pressure. Figure 10 chromium data include respective P(psi)$-T_{react}$(°R)$-T_{diff}$(°R) triplets of 10–1800–2200; 100–2000–2400; 1000–2350–2800; 2500–2400–3000; 5000–2600–3000; 15,000–2800–3200; and 30,000–3000–3400. Figure 14 gun steel data includes respective P(psi)$-T_{react}$(°R)$-T_{diff}$(°R) triplets of 10–800–1600; 100–1150–2000; 1000–1200–2400; 2500–1350–2600; 5000–1400–2800; 15,000–1550–3000; and 30,000–1600–3000.

For MACE analysis, radiation effects from emissivity and absorptivity are not a factor until about 4000°R. Using a past MACE code illustration, a considerable amount of analysis has been performed on re-entry heating of graphite heat shields in air using carbon–air kinetic rate functions. Based on analysis and test data, it has been shown that below 1500°R the graphite does not react with the flow, and above 3000°R the system is in equilibrium, resulting in $T_{react} = 1500$°R and $T_{diff} = 3000$°R. Based on these results, the cubic transition function was formulated to relate the ratio of the kinetic reaction rate to the equilibrium rate when the surface temperature is between T_{react} and T_{diff}. The carbon–air kinetic rate function plots temperature (°R) against $\dot{M}/\dot{M}_{diff}$ and begins at 1500°R as an exponential kinetic curve that is not diffusion-limited, and transitions to a diffusion-limited (equilibrium) curve at about 2700°R. Each chemical system requires additional analysis and possibly test data to determine the appropriate T_{react} and T_{diff}. Because these quantities are not known for the problem of interest, the MACE study performed a parametric analysis of T_{react} and T_{diff} using equilibrium enthalpies.

At this point in code development, single-shot comparisons of wall material erosion are preferable to absolute calculations. For the given example, predicted single-shot thermochemical wall erosion

is compared, where both interfacial and exposed surface gun steel eroded more than 1×10^6 times faster than chromium at either of the two chosen axial positions.

To date, the U.S. Army Armament Research, Development, and Engineering Center's investment in this gun-erosion technology area has yielded the first practical gun-erosion modeling code. Gun-erosion modeling can reduce the cost of designing extended-life high-performance gun systems that push materials' technology limits and explain gun erosion-related phenomenon.

Current gun-erosion code improvement projects include tedious-step automation, master-control module unification, dual chemical equilibrium module combination, time-dependent boundary-layer development, and mass transfer phase-component separation.

References

[1]von Karman, T., "Sorbonne Lectures," Sorbonne, France, 1951–1952; also Princeton University Lectures, 1953; "Fundamental Approach to Laminar Flame Propagation," *AGARD Selected Combustion Problems*, Butterworths, London, 1954; "Fundamental Equations in Aerothermochemistry," *Proceedings of the 2nd AGARD Combustion Colloquium*, AGARD, 1955.

[2]Reshotko, E., and Cohen, C. B., "Heat Transfer at the Stagnation Point of Blunt Bodies," NACA TN 3513, JuIy 1955.

[3]Cohen, C. B., Bromberg, R., and Lipkis, R. P., "Boundary Layers with Chemical Reactions Due to Mass Additions," Ramo-Wooldridge Corp., GM-TR-268, Los Angeles, Oct. 1957.

[4]Denison, M. R., and Dooley, D. A., "Combustion in the Laminar Boundary Layer of Chemically Active Sublimators," Aeronutronic Systems, Inc., Publication C-110, Glendale, CA, Sept. 1957.

[5]Lees, L., "Convective Heat Transfer with Mass Addition and Chemical Reactions," *Proceedings of the 3rd AGARD Combustion Colloquium*, Pergamon, New York, 1958; also *Recent Advances in Heat and Mass Transfer*, McGraw–Hill, New York, 1961, pp. 161–207.

[6]*JANNAF Thermochemical Tables*, Thermal Research Lab., National Bureau of Standards, Dow Chemical Co., Midland, MI, 1971.

[7]"Aerotherm Axi-Symmetric Transient Heating and Material Ablation Computer Program (ASTHMA 3)," Acurex Corp., Aerotherm Div., Mountain View, CA, 1972.

[8]"Conduction Ablation Reaction Erosion Program (CARE)," TRW Defense and Space Systems Group, Redondo Beach, CA, 1973.

[9]"Passive Nosetip Technology Program (PANT I&II) for RV Erosion and Ablation: Erosion Shape Computer Code (EROS), ABRES Shape Change Code (ASCC), Updated ABRES Shape Change Code (ASCC 80), Maneuvering ABRES Shape Change Code (MASCC), Controlled Shaping for Ablation/Particle Erosion Code (COSHAPE), and Shape-Stable Nosetip Performance Prediction Code (ASCC85)," Acurex Corp., Aerotherm Div., Mountain View, CA, 1974–1986.

[10]"Erosion Resistant Nosetip Technology Program (ERNT)," TRW Defense and Space Systems Group, Redondo Beach, CA, 1975.

[11]Moody, H. L., Smith, D. H., Haddock, R. L., and Dunn, S. S., "Tungsten and Molybdenum Ablation Modeling for Reentry Applications," *Proceedings of the AIAA 13th Aerospace Sciences Meeting*, AIAA, New York, 1975.

[12]Nickerson, G. R., "A Steady State Model for the Thermochemical Ablation Performance of Binary Materials," Prototype Development Associates, Inc., TM 5003-00-01, Santa Ana, CA, 1975.

[13]Nickerson, G. R., "Erosion Resistant Materials for MaRV Application," Prototype Development Associates, Inc., 1038-00-05, Santa Ana, CA, April 1976.

[14]Crose, J., "Reentry Vehicle Materials Technology Program (REVMAT)," Prototype Development Associates, Inc., Santa Ana, CA, 1976.

[15]Gomez, A. V., "Passive Transpiration Cooling Analysis (PCOOL-1D) for Chemically Reacting Metallic Ablators," TRW Defense and Space Systems Group, 28266-6001-RU-00, Redondo Beach, CA, March 1976.

[16]Sherman, M. M., and Smith, D. H., "A Monte Carlo Statistical Uncertainty Analysis Method for Nosetip Recession Predictions," *Proceedings of the AIAA/ASME 2nd Thermophysics and Heat Transfer Conference*, AIAA, New York, 1978; also Prototype Development Associates, Inc., TM, Santa Ana, CA, 1978.

[17]Gordon, S., and McBride, B., "Computer Program for Calculation of Complex Chemical Equilibrium Compositions, Rocket Performance, Incident and Reflected Shocks, and Chapman-Jouguet Detonations (CET)," NASA SP-273, March 1971.

[18]Levine, J., "Transpiration and Film Cooling Boundary Layer Computer Program (MABL)," *Finite Difference Computer Program for Solving Turbulent Boundary Layer Equations with Equilibrium Chemistry*, Vol. 1, N72-19312, 1971.

[19]Murphy, A. J., Chu, E. K., and Kesselring, J. P., "AFRPL Graphite Performance Prediction Program," *Recommendations for a Standardized Analytic Procedure for MX Missile Nozzle Throat Recession Calculations*, Vol. 1, U.S. Air Force Research Propulsion Lab., TR-75-59, Edwards AFB, CA, 1975; also Aerotherm Div., Acurex Corp., TM 75-143, Mountain View, CA, 1975.

[20]Coats, D. E., Levine, J. N., Nickerson, G. R., Tyson, T. J., Cohen, N. S., Harry, D. P., and Price, C. H., "A Computer Program for the Prediction of Solid Propellant Rocket Motor Performance," Ultrasystems, Inc., CPIA Publication 246, Irvine, CA, July 1975.

[21]Nickerson, G. R., Coats, D. E., and Hermsen, R. W., "A Computer Program for the Prediction of Solid Propellant (SPP) Rocket Motor Performance," Vols. 1 and 3, Software and Engineering Associates, Inc., Santa Ana, CA, 1981.

[22]Abbett, M., and Chiba, Z., "Particle Impact Erosion Program (PIE) for Rocket Nozzle Recession Predictions: Chamber Flowfield Code (CFC) and Charring Material Ablation-Erosion Code (CMAE)," *15th JANNAF Performance Standardization Subcommittee Meeting*, Aerotherm Div., Acurex Corp., Mountain View, CA, 1982, pp. 135–138.

[23]Moody, H. L., Haddock, R. L., and Miyazawa, E. T., "Rocket Nozzle Thermal Analysis Program: Rocket Nozzle Heating and Recession Code (ROHARE) and Rocket Nozzle Shape Change, Erosion and Conduction Code (ROSEC)," PDA Engineering, Santa Ana, CA, 1983.

[24]Coats, D. E., Nickerson, G. R., Dang, A. L., Dunn, S. S., and Kehtarnavaz, H., "The Solid Propellant Rocket Motor Performance Computer Program (SPP)," Version 6.0, Software and Engineering Associates, Inc., Carson City, NV; also *Proceedings of the AIAA/SAE/ASME 23rd Joint Propulsion Conference*, AIAA, New York, 1987.

[25]Coats, D. E., Berker, D. R., and Dunn, S. S., "Boundary Layer Study: JANNAF Standard TDK/BLM Code; the Parabolized N/S Two-Phase Finite Rate Chemistry Code (VIPER); and the Modified Creare CFD Program (Fluent)," Software and Engineering Associates, Inc., Carson City, NV, 1990.

[26]Nickerson, G., Berker, D., Coats, D., and Dunn, S., "Two-Dimensional Kinetics (TDK) Nozzle Performance Computer Program," Software and Engineering Associates, Inc., NAS 58-39048, Carson City, NV, March 1993.

[27]Dunn, S. S., "Materials Ablation Conduction Erosion Program (MACE)," Software and Engineering Associates, Inc., SEA 89-01, Carson City, NV, March 1989.

[28]Freedman E., "BLAKE—A Thermodynamic Code Based on Tiger: User's Guide and Manual," U.S. Army Ballistic Research Lab., TR ARBRL-TR-02411, Aberdeen Proving Ground, MD, Feb. 1982.

[29]Gough, P., "The XNOVAKTC Code," Paul Gough Associates, Portsmouth, NH, 1990.

[30]Garn, P., *Thermoanalytical Methods of Investigation*, Academic, New York, 1965.

[31]Lodding, W., *Gas Effluent Analysis*, Marcel Dekker, New York, 1967.

[32]Margrave, J., *The Characterization of High-Temperature Vapors*, Wiley, New York, 1967.

[33]Benson, S., *Thermochemical Kinetics—Methods for the Estimation of Thermochemical Data and Rate Parameters*, Wiley, New York, 1968.

[34]Fast, J., *Interaction of Metals and Gases*, Academic, New York, 1965.

[35]Kofstad, P., *High-Temperature Oxidation of Metals*, Wiley, New York, 1966.

[36]Picard, J., Ahmad, I., and Bracuti, A., *Proceedings of the Tri-Service Gun Tube Wear and Erosion Symposiums*, U.S. Army Armament Research, Development, and Engineering Center, Dover, NJ, 1970, 1972, 1977, and 1982.

[37]Vassallo, F., and Brown, W., "Shock Tube Gun Melting Erosion Study," Calspan Corp., VQ-6123-D, Buffalo, NY, Aug. 1979.

[38]Chufarov, G. I., et al., "Thermodynamics of the Oxidation of Metals," *Surface Interactions Between Metals and Gases*, edited by V. I. Arkharov and K. M. Gorbunova, translated by Consultants Bureau, New York, 1966, pp. 5–20.

[39]Argent, B. B., and Birks, N., "Rate-Limiting Reactions in High Temperature Oxidation Processes," *High Temperature Materials—The Controlling Physical Processes*, Oliver and Boyd, Edinburgh, 1968.

[40]Kamdar, M., Brassard, T., and Campbell, A., "A Metallographic Study of White Layers in Gun Steel," ARLCB-TR-78012, Benet Weapons Lab., Watervliet, NY, Aug. 1978.

[41]Morphy, C., and Fisher, E., "The Role of Carburization in Gun Barrel Erosion and Cracking," Calspan Corp., Buffalo, NY, 1981.

[42]Fisher, R., Szirmae, A., and Kamdar, M., "Metallographic Studies of Erosion and Thermo-Chemical Cracking of Cannon Tubes," U.S. Army Large Caliber, Benet Labs., ARLCB-TR-83022, Watervliet, NY, May 1983.

[43]Kamdar, M., and Venables, J., "Characterization of Bore Surface Layers in Gun Barrels," U.S. Army Large Caliber, Benet Labs., ARLCB-TR-84041, Watervliet, NY, Dec. 1984.

[44]Alkidas, A., Morris, S., Christoe, C., Caveny, L., and Summerfield, M., "Erosive Effects of Various Pure and Combustion-Generated Gases on Metals—Part II," U.S. Army Materials and Mechanics Research Center, AMMRC-CTR-77-25, Watertown, MA, Oct. 1977; also AMMRC-CTR-75-23, Pt. I, Oct. 1975.

[45]Johnson, J., Caveny, L., and Summerfield, M., "Hot Gas Erosion of Gun Steel," *Proceedings of the Tri-Service Conference on Corrosion*, Battelle Lab., Columbus, OH, 1979, pp. 187–201.

[46]Krishnan, G., Scott, A., Wood, B., and Cubicciotti, D., "Effect of Transient Combustion Species on 4340 Steel," U.S. Army Research Office, ARO-15181.1-MS, Research Triangle, NC, May 1979.

[47]Fisher, E., and Morphy, C., "The Role of Oxygen in Gun Barrel Erosion and Cracking—A Shock Tube Gun Investigation," Ballistics Research Lab., ARBRL-CR-00427, Aberdeen, MD, April 1980.

[48]Morphy, C., and Fisher, E., "Gas Chemistry Effects on Gun Barrel Erosion—A Shock Tube Gun Investigation," Ballistics Research Lab., ARBRL-CR-00481, June 1982.

[49]Lin, S., "Auger Electron Spectroscopic Study of Gun Tube Erosion and Corrosion," *Applications of Surface Science*, Vol. 15, No. 1–4, 1983, pp. 149–165.

[50]Lin, S., "Chemical Constituents of Eroded Gun Surfaces," *Applications of Surface Science*, Vol. 21, No. 1–4, 1985, pp. 112–124.